How do ocean warm anomalies favor the aggregation of deep convective clouds?

Sara Shamekh, Caroline Muller, Jean-Philippe Duvel, Fabio d'Andrea

How do ocean warm anomalies favor the aggregation of deep convective clouds?

Sara Shamekh*

Laboratoire de Météorologie Dynamique/IPSL, École Normale Supérieure, PSL Research University, CNRS, Paris, France

Caroline Muller

Laboratoire de Météorologie Dynamique/IPSL, École Normale Supérieure, PSL Research University, CNRS, Paris, France

Jean-Philippe Duvel

Laboratoire de Météorologie Dynamique/IPSL, École Normale Supérieure, PSL Research University, CNRS, Paris, France

Fabio D'Andrea

Laboratoire de Météorologie Dynamique/IPSL, École Normale Supérieure, PSL Research University, CNRS, Paris, France

Corresponding author address: Laboratoire de Météorologie Dynamique, École Normale Supérieure, 24 Rue Lhomond, 75005 Paris, France

E-mail: shamekh@lmd.ens.fr

ABSTRACT

We investigate the role of a warm sea-surface temperature (SST) anomaly (hot-spot of typically 3 K to 5 K) on the aggregation of convection using cloud resolving simulations in a non-rotating framework. It is well known that SST gradients can spatially organize convection. Even with uniform SST, the spontaneous self-aggregation of convection is possible above a critical SST (here 295 K), arising mainly from radiative feedbacks. We investigate how a circular hot-spot helps organize convection, and how self-aggregation feedbacks modulate this organization. The hot-spot significantly accelerates aggregation, particularly for warmer/larger hot-spots, and extends the range of SSTs for which aggregation occurs, however at cold SSTs (290 K) the aggregated cluster disaggregates if we remove the hot-spot. A large convective instability over the hot-spot leads to stronger convection and generates a large-scale circulation which forces the subsidence drying outside the hot-spot. Indeed, convection over the hot-spot brings the atmosphere towards a warmer temperature. The warmer temperatures are imprinted over the whole domain by gravity waves and subsidence warming. The initial transient warming and concomitant subsidence drying suppress convection outside the hot-spot, thus driving the aggregation. The hot-spot induced large-scale circulation can enforce the aggregation even without radiative feedbacks for hot-spots sufficiently large/warm. The strength of the large-scale circulation, which defines the speed of aggregation, is a function of the hot-spot fractional area. At equilibrium, once the aggregation is well established, the moist convective region with upward mid-tropospheric motion, centered over the hot-spot, has an area surprisingly independent of the hot-spot size.

1. Introduction

In the tropics, convection can be organized by synoptic dynamical systems such as equatorial waves or tropical depressions, but it may also have its own organization sources such as in squall lines, or more generally in mesoscale convective systems. Organized convection is associated with extreme weather conditions (Houze 2004), and can strongly impact the hydrological cycle and the top-of-atmosphere radiation budget (Tan et al. 2015; Tobin et al. 2012). For large-scale processes such as the Madden Julian Oscillation, the aggregation of the convection may generate non-linear effects modifying the average circulation at basin scale (Bellenger et al. 2009). However, the physical processes responsible for the mesoscale organization of convection are still not clearly identified and are typically not specifically accounted for in global climate models (GCMs) (Mapes and Neale 2011).

The spontaneous clustering of convective clouds in simulations in idealized settings, typically non-rotating Radiative-Convective Equilibrium (RCE), provides a manageable framework to gain fundamental understanding of the physical processes at stake. Non-rotating RCE is an idealization of the tropical atmosphere where the Earth's rotation is neglected, a reasonable approximation in the deep tropics where the Coriolis parameter is small, and where the large-scale circulation (larger than the model domain) is neglected. In other words, in RCE, there is no advection of energy into or out of the domain. Thus in the domain mean, surface latent and sensible heat fluxes are in balance with the net radiative cooling of the atmosphere (top-of-atmosphere minus surface).

In the tropics, such equilibrium is only reached at large, thousands of kilometers scales (Muller and O'Gorman 2011). The idealized framework of RCE has proven to be useful to study and improve our understanding of numerous aspects of tropical convection, including precipitation extremes (Muller et al. 2011; Muller 2013), entrainment (Romps 2010), cold pools (Tompkins

2001a), atmospheric thermodynamics (Pauluis and Held 2002) or rain evaporation (Muller and Bony 2015). Notably, it has led to the discovery of the remarkable ability of deep convection to spontaneously cluster in space despite homogeneous forcing in cloud-resolving models (CRMs). These are models with sufficient kilometr-scale horizontal resolutions to resolve the main features of deep convection, instead of parameterizing them.

Typical RCE simulations with homogeneous forcing (doubly-periodic geometry, square domain, constant sea-surface temperature (SST) in space and time) reach a statistically steady state in which convection and clouds are somewhat randomly distributed. But under certain conditions, including large domains, deep clouds aggregate into a region of the domain, surrounded by a dry environment devoid of deep convection. This phenomenon, known as self-aggregation in the literature (see, e.g., Wing et al. (2017) for a review), leads to an equilibrium state with dry and warm mean thermodynamic profiles, and enhanced outgoing longwave radiation (OLR) to space (Bretherton et al. 2005; Tobin et al. 2012). Since its discovery in idealized CRM simulations, the self-aggregation of deep convection has been confirmed to occur in more realistic settings (Holloway 2017) and even in GCMs with parameterized convection (Coppin and Bony 2015).

Radiative feedbacks are believed to be key for self-aggregation, at least at temperatures observed in the tropical atmosphere (Wing et al. 2017). It is the circulation generated by the differential longwave radiative cooling rates between dry (strong cooling) and moist (little cooling or even warming) regions which is believed to trigger and maintain the convective aggregation (Bretherton et al. 2005; Muller and Held 2012). Strong cooling in dry regions yields subsidence down to low levels, and a near-surface flow from dry to moist regions. Such a process was already proposed by Gray and Jacobson (1977) to explain the observed reinforcement of large convective systems at the end of the night. This circulation transports near-surface high moist static energy (MSE) from dry to moist regions. This MSE upgradient transport maintains high MSE in the moist region,

helping to maintain deep convection there. In fact, in the CRM used in this study (System for Atmospheric Modeling, or SAM (Khairoutdinov and Randall 2003)), there is no self-aggregation without interactive radiation (unless the evaporation of rain is artificially suppressed (Muller and Bony 2015), a particular case which will not be discussed here). Because of the idealized settings in which self-aggregation was discovered, its relevance to the real world is still debated. Notably, the aforementioned CRM studies used spatially and temporally constant and uniform sea-surface temperatures (SSTs).

The impact of SST anomalies on deep convection has already been widely studied in the literature (Tompkins 2001b; Kuang 2012; Ramsay and Sobel 2011; Sobel and Bretherton 2000). Tompkins (2001b) found in particular that a sudden inverting of an imposed SST anomaly leads to the migration of the convective clusters over the warm anomaly. The migration of aggregated convective clusters over warm anomalies has been confirmed by other studies which used a slab ocean in order to have interactive SSTs (Coppin and Bony 2015; Grabowski 2006). Using a single column model (SCM) and CRM, Ramsay and Sobel (2011) and Wang and Sobel (2011) showed that precipitation rate increases over local warm SSTs and is determined by the temperature anomaly rather than by the mean SST. Daleu et al. (2017) confirmed this result using two adjacent SCMs with different SSTs. The SST difference, if large enough, can suppress convection in the cold column and strengthen it in the warm column. Notably, SST gradients can generate a large-scale circulation that can lead to a migration of deep convection towards the warmest SST.

Another type of surface temperature anomalies are tropical islands with different surface properties, which act as a surface forcing and change the intensity of convection (Crook 2001; Beringer and Tapper 2002) and thermal structure of the atmosphere (Cronin et al. 2014). Rainfall over tropical islands is larger than over the surrounding ocean (Cronin et al. 2014; Sobel et al. 2011; Qian 2008; Wang and Sobel 2017), however the strength of the thunderstorms and precipitation

depends on several factors such as the size of the islands, wind speed and direction and the island's topography (Wang and Sobel 2017; Crook 2001). Convective events over tropical islands show large diurnal variations, however they build up an average ascent (Cronin et al. 2014) .

Ocean mesoscale eddies (Chelton 2011) can also be associated with SST anomalies reaching a few degrees in cold core cyclonic eddies or warm core anticyclonic eddies. These persistent ocean eddies have a typical radius varying with latitude, from a hundred to a few hundreds of kilometers in the tropics ($\pm$ 20° latitude), to around 50 km or less in mid-latitudes. As a surface forcing, eddies can impact the atmosphere locally (Sugimoto et al. 2017) by enhancing low level convergence and thus convective precipitation. Potentially, the eddies change the cloudiness and wind field which can impact the large scale circulation .

Whether and how such persistent SST anomalies, as an external forcing, can favor or suppress the aggregation of convection is, to our knowledge, still not well covered in the literature. In this paper, we investigate the aggregation response to an idealized, circular SST anomaly referred to as a "hot-spot'. We must emphasize that the aggregation forced by a hot-spot, when it is the case, is not anymore "self-aggregation" but rather a forced aggregation. Of particular interest are the following questions:

- How does the presence of an ocean hot-spot modify or enforce the aggregation process of the deep convection? And how does this modification depend on the hot-spot radius and temperature anomaly?

- How does the hot-spot impact the large-scale circulation?

- In the presence of a hot-spot, how does the aggregation physics differ from the self-aggregation ones; specifically, does aggregation disappear in the absence of radiative feedbacks (known to be crucial for self-aggregation over homogeneous SST)?

The next section, § 2, describes the cloud-resolving model used and the experimental setup, as well as the metrics used to measure (self-)aggregation. § 3 investigates the impact of the hot-spot on convective aggregation, and the sensitivity to hot-spot properties. § 4 investigates whether radiative feedbacks are still necessary for aggregation to occur when a hot-spot is present. Additionally, we derive a simple, two-box model to help comparison between the onset of self-aggregation and aggregation. In § 5 we briefly discuss the equilibrium phase, once aggregation has occurred. Conclusions are given in § 6.

2. Model description and simulation design

a. Cloud-resolving model

The CRM used is the model System for Atmospheric Modeling (SAM) version 6.11.1 (Khairoutdinov and Randall 2003). This model solves the anelastic equations of conservation of momentum, water (with 6 species present in the model, water vapor, cloud liquid, cloud ice, precipitating rain, precipitating snow, and precipitating graupel), and energy. The relevant energy for moist convection is the moist static energy, as it is conserved (approximately, i.e. neglecting viscous and subgrid-scale effects) under adiabatic processes including the phase change of water. More precisely in this model, the so-called "frozen" MSE is conserved during moist adiabatic processes, including the freezing of precipitation. The frozen MSE is given by

$$MSE = c_p T + gz + L_v q_v - L_f q_{ice}, \tag{1}$$

with the specific heat capacity of air at constant pressure c_p, temperature T , gravity g, height z, latent heat of evaporation L_v, water vapor mixing ratio q_v, latent heat of fusion L_f, and mixing ratio of all ice phase condensates q_{ice}.

The subgrid-scale turbulence is modeled using a Smagorinsky-type parameterization, and we use the 1-moment microphysics formulation, following Bretherton et al. (2005) and Muller and Held (2012). Bulk formulae are used to compute surface fluxes. Further information about the model can be found in Khairoutdinov and Randall (2003).

Most simulations use interactive radiation, using the radiation code from the National Center for Atmospheric Research (NCAR) Community Atmosphere Model version 3 (CAM3; (Collins et al. 2006)). For simplicity, we neglect the diurnal cycle and use the daily mean incoming solar insolation of 413 W m^{-2} (same setting as Tompkins and Craig (1998)). Studies of self-aggregation over the ocean with a diurnal cycle show that, quantitatively, a diurnal cycle can change the strength of the hydrological cycle, increasing the daily precipitation range. But qualitatively, beyond this daily modulation of amplitude, it does not seem to affect the fact that deep convection self-aggregates or not.

In some simulations, radiative feedbacks are turned off by homogenizing radiative cooling rates horizontally, at each height and time step, following Muller and Held (2012). Note that in that case, the domain average radiative cooling rates can still evolve in time.

b. Experimental setup

The model domain is square, doubly-periodic in both horizontal directions x and y. We run simulations with two domain sizes, (288 km)^2 and (576 km)^2 (except for one simulation shown in Figure 1 with a smaller (96 km)^2 domain). The horizontal resolution is 3 km and the vertical grid spacing increases gradually with height, with the first level at 25 m and a resolution of 50 m close to the sea surface, reaching a vertical resolution of 500 m in the mid troposphere. There are 64 vertical levels which span 27 km in the vertical. This includes a sponge layer in the upper third of the domain (from $z = 18$ km to 27 km) where the wind is relaxed to zero in order to reduce gravity

wave reflection and buildup. No large-scale forcing or wind is imposed. We neglect the Earth's rotation, a reasonable approximation in the tropics where the Coriolis parameter is small.

The initial conditions for the different mean SSTs (horizontal mean SSTs in our simulations with and without hotspot) are obtained from a smaller domain run with the corresponding SST at RCE ($(96\ \text{km})^2$ run to 50 days), then using time and domain averaged profiles of the last 5 days. We run two different types of simulations: simulations with a uniform and constant sea surface temperature that we refer to as ocean experiments, and simulations with a warm temperature anomaly referred to as hot-spot experiments. The hot-spot is a circular area with a higher temperature than the surrounding ocean, located at the center of the domain. A given hot-spot simulation will be defined by its temperature anomaly dT and its radius R so that, for example, simulation dT5R60 is for a hot-spot with a temperature anomaly of 5 Kelvin and a radius of 60 km. The upper two panels of Figure 1 show snapshots of near-surface air temperature and cloud water for two simulations with a different domain size and hot-spot radius. This illustration shows that, although there is some organization of convection on the small domain in the presence of a hot-spot, the self-aggregation of convection surrounded by extremely dry air only occurs in the large-domain simulation. This is well captured by the metrics used to quantify the degree of aggregation described next and shown in Figure 1c. In the following, in both ocean and hot-spot experiments, we also investigate the role of radiative feedbacks by repeating some simulations with homogenized radiation.

c. Aggregation metrics

The convective aggregation is associated with progressive drying of the dry environment surrounding deep clouds, and progressive moistening of the moist region where deep convection occurs. This leads to increased horizontal moisture variability. Thus a common index for self-aggregation is the difference between the 75^{th} and 25^{th} percentiles of precipitable water, ΔPW_{75-25}

(Muller and Held 2012; Muller and Bony 2015). Since here we will compare simulations with different SSTs, we will use precipitable water normalized by the saturation water vapor path, i.e. we will use column relative humidity *CRH* (Wing and Cronin 2016),

$$CRH = \frac{\int q_v \rho dz}{\int q_{v,sat} \rho dz}, \tag{2}$$

where $q_{v,sat}$ denotes the saturation water vapor mixing ratio, ρ density and the vertical integration done over the troposphere. Our aggregation index is the difference between the 75^{th} and 25^{th} percentiles of column relative humidity, ΔCRH_{75-25}. Figure 1 illustrates the increase of this index (bottom panel) in the simulation that aggregates (middle panel).

In SAM, self-aggregation has been shown to start with the strengthening and the expansion of a dry patch, becoming drier and larger. This dry region, devoid of deep convection, was sometimes referred to as the "radiative dry pool" (Coppin and Bony 2015; Zuidema et al. 2017), as it is believed to be radiatively driven. The dry patches are thus of primary importance, as the self-aggregation of convection can eventually result from the confinement of the deep convection in a restricted region because of the expansion of a dry patch in our doubly-periodic geometry. In the following, the dry patch is defined as the area where the *CRH* is below the 25^{th} percentile.

3. Hot-spot impact on aggregation of deep convection

Here, we first investigate how the presence of a hot-spot impacts the aggregation of convection in the presence of radiative feedbacks. Of particular interest is whether the aggregation is faster, and whether the deep convection area ends up being localized over the hot-spot.

a. Results without and with hot-spot at different SSTs

The upper row of Figure 2 shows the *CRH* maps in a control ocean experiment with a mean SST of 300 K at different times started from homogeneous conditions. We observe the typical

evolution of self-aggregation: the appearance of a dry patches after a few days (day 11) and thus the extension and merge of these dry patches into a single patch (day 31). At day 41, the *CRH* in the dry region reaches extremely low values, and convection and moisture are confined to a small part of the domain. After day 41, the moist patch shrinks to a narrow region surrounded by a very dry environment. The increased spatial moisture variability between dry and moist regions, largely due to enhanced drying, is also visible in ΔCRH_{75-25} (Figure 3a). It increases up to day 40 and then starts to decrease slowly. With further progress of aggregation, the high CRH region shrinks to a circular area smaller than 25 percent of the domain, thus CRH_{75} decreases, leading to the decrease of the aggregation index.

Self-aggregation over fixed SSTs is known to depend on the domain mean SST. Using the same SAM model, Wing and Emanuel (2014) find that warm SSTs favor aggregation, while Coppin and Bony (2015) find in a GCM that self-aggregation is surprisingly favored both for SSTs larger than 295K or smaller than 285K. In very cold snowball simulations, aggregation can also occur (Abbot 2014), though in that case a weak wind shear can prevent the aggregation. The exact relation between an average SST and the self-aggregation response is hence still unclear, but the general consensus is that self-aggregation is favored at warm SSTs (Emanuel et al. 2014). Consistently, we find that for a colder SST of 290 K aggregation does not occur, and that the aggregation speed increases regularly with the SST for SST values between 295 K and 305 K (Figure 3a).

Simulations with the same mean SST, but with different hot-spot characteristics are performed to analyze the role of the SST anomaly on the convective aggregation. Here the domain-mean SST is kept constant at 300 K in order to isolate the effect of the hot-spot temperature anomaly. Consequently, the surrounding ocean temperature is slightly lower than 300 K in the hot-spot simulations. However, it has been argued in previous studies (Ramsay and Sobel (2011); Wang and Sobel (2011)) that the control parameter is the SST anomaly (dT) and not the absolute SST,

at least for a reasonable temperature change. Figure 2b shows the hot-spot experiment dT5R60 (dT=5 K and R=60 km). Spatially, the main aspects of aggregation in the presence of a hot-spot are similar to the ocean experiment, with a progressive expansion of dry regions. The aggregation is however much faster with the hot-spot and the convection is eventually organized over or near the hot-spot. Note that the location of the aggregation is not stable, and whether the aggregated convective cluster stays over the hot-spot depends on hot-spot radius and temperature. If the hot-spot is sufficiently large and/or warm, it sustains the convective cluster over it, otherwise, it does not necessarily stay over the hot-spot after its formation. We will discuss this in more detail in § 5.

Looking at the aggregation index (Figure 3b), the maximum aggregation is in fact reached after only 10 days in dT5R60 compared to 40 days in the ocean simulation at 300K. Thus, the presence of a hot-spot may accelerate the aggregation by a factor of 4. However, the aggregation is much faster with a hot-spot. When the aggregation is fully reached, the aggregation index is fairly comparable between the simulations with and without a hot-spot. The hot-spot temperature anomaly plays a significant role in accelerating or enforcing the aggregation, as can be seen in Figure 3b. For dT5R60 the aggregation index reaches a maximum after only 10 days while for dT3R60 the maximum is reached in 20 days. Thus, the aggregation speed is favored by larger hot-spot temperature anomaly. The hot-spot size also plays a role with a maximum aggregation index reached in less that 10 days for dT3R120. Therefore, the larger the hot-spot, the faster the aggregation. Note though that for very large hot-spots relative to the domain size (see below), this can not hold anymore. A hot-spot can also extend the range of SSTs for which an aggregation occurs. For example, with an average SST of 290 K, there is no self-aggregation for uniform SST (3a), but the dT5R60 experiment at 290 K aggregates even faster than uniform ocean simulations at 305 K. (3b).

b. Development of a large-scale circulation

Here, we hypothesize that the presence of the hot-spot favors and accelerates the formation of a large-scale circulation that triggers the onset of convective aggregation, and thus extends the range of SSTs at which aggregation occurs.

To explain the acceleration of aggregation with a hot-spot, we look at virtual potential temperature (θ_v) anomaly. In the free troposphere, gravity waves remove horizontal θ_v anomalies very efficiently (Bretherton and Smolarkiewicz 1989; Ruppert and Hohenegger 2018) so that θ_v profile above the boundary layer is fairly uniform over the domain especially when it is averaged over a few hours. So the main source of instability is the buoyancy anomaly in the boundary layer. Figure 4 shows θ_v anomaly averaged over the boundary layer for the ocean experiment at SST=300 K at day 31 and the hot-spot experiment dT5R60 with a mean SST equal to 300 K at day 11 (Figure 2 shows the CRH evolution for these two simulations). We compare these two days as the aggregation index and the fraction of area covered with low (high) CRH are comparable between the two simulations. In general there is a positive θ_v anomaly in moist areas (except directly below clouds where cold pools result from the partial evaporation of rain), that enforces convergence of low-level air toward the moist area. Consistent with the faster aggregation, the θ_v anomaly is larger over the hot-spot. θ_v depends on both temperature and water vapor. In both the ocean and hot-spot simulations, the moisture contribution to the θ_v anomaly in moist regions is positive. But the temperature contribution is smaller in the ocean experiment. In the hot-spot simulations, over the hot-spot, both temperature and moisture have a positive contribution to θ_v resulting in a slightly larger θ_v anomaly and a stronger instability over the hot-spot that leads to stronger convection.

The corresponding pressure gradient at the first few levels enforces a convergence of moisture toward the moist region. With a hot-spot, the pressure gradient is larger and it stays over the hot-

spot. This convergence favors convection over the hot-spot by transporting low level moist air and by providing energy to lift the air above the hot-spot. Additionally, the convergence of moisture removes moisture from the environment and inhibits convection there. This process (low-level transport of moisture toward the moist region) thus seems common to both self-aggregation and aggregation but is stronger in the latter case. There is a difference though: in aggregation with a hot-spot, it is the strength of the upward mass flux over the hot-spot which seems to control the large-scale circulation and thus the aggregation speed. Ascent over the hot-spot forces compensating subsidence in the environment, which dries the troposphere and results in further suppression of convection there and enhancement of moisture transport toward the hot-spot. This upward motion over the hot-spot and thus subsidence in the environment, is partly a consequence of our periodic boundary conditions, and it builds up a large scale circulation that accelerates the aggregation. Instead, with self-aggregation, it has been hypothesized that it is the subsidence in dry regions which initiates and controls the large-scale circulation, and thus the self-aggregation speed. This development of a large-scale circulation will be further investigated in the next section.

A natural question then, is whether the large-scale circulation enforced by the hot-spot can be maintained even in the absence of a hot-spot, solely by internal self-aggregation feedbacks. The sensitivity of self-aggregation to initial conditions is well documented. Aggregated states that are imposed as initial conditions can persist, even under conditions which do not favor the spontaneous self-aggregation from homogeneous initial conditions (Khairoutdinov and Emanuel 2010; Muller and Held 2012). To investigate whether the hot-spot aggregation exhibits hysteresis, we repeat the dT5R60 with SST=290 K simulation, which does not self-aggregate without a hot-spot, for 30 days, and then remove the hot-spot (by simply setting dT to zero) and run for another 30 days. The aggregated cluster spreads over the domain and disaggregates. Therefore the aggregation is not maintained without the hot-spot in this case.

4. Convective aggregation without radiative feedbacks

a. Hot-spots with or without radiative feedbacks

Radiative feedbacks have been shown by many studies to be necessary for convective self-aggregation, at least for typical tropical SSTs around 300 K (Wing et al. 2017). The balance between radiative cooling and subsidence warming in dry regions (Mapes 2001) creates a positive feedback that results in radiatively enhanced subsidence and drying of already dry regions. Sensitivity studies show that removing radiative feedbacks, by homogenizing radiative cooling rates, prevents the self-aggregation. Here we test the occurrence of aggregation without radiative feedbacks in hot-spot experiments, listed in Table 1.

Comparing the dT5R60 simulation with (Figure 2b) or without (Figure 5a) radiative feedbacks, we see that homogenizing the radiation prevents aggregation for a hot-spot radius of 60 km. However, increasing the hot-spot radius to 70 km (Figure 5b) yields aggregation even without radiative feedback. For R=70 km, the aggregation is very slow, but it becomes much faster at larger radius (Figure 6). It is worth noting that simulations with R=70 and 80 km give a banded aggregation. For larger hot-spots, a circular aggregation of the convection develops in a few days, with a maximum aggregation index reached in less than 10 days with R=180 km. This is fast compared to typical overturning time scale of the atmosphere (Grabowski and Moncrieff 2001), suggesting that the circulation between dry and moist regions is greatly accelerated by the presence of the SST anomaly. By reducing this anomaly to 3K instead of 5K, there is no convective aggregation, even for a radius of 80 km (Figure 6). A persistent SST anomaly can thus clearly trigger a convective aggregation in SAM, even without radiative feedbacks. This aggregation requires a minimum size and amplitude of the SST anomaly, and is faster for warm and large hot-spots. In order to clarify

the physical processes responsible for convective aggregation in that case, we look in the next section at the large-scale circulation in more detail, in particular the subsidence in the dry regions.

Note that because we keep the mean SST constant, changing the hot-spot radius R and temperature anomaly dT, also changes the temperature outside the hot-spot and the absolute temperature of the hot-spot (both reduced to keep the domain mean SST constant). To verify that the leading order parameter determining the onset and speed of aggregation is the hot-spot temperature anomaly dT, not its absolute temperature, we redo some of the simulations keeping the temperature equal to 300 K outside the hot-spot, and simply adding a hot-spot with dT=5 K to the domain (so that the domain mean SST is now larger than 300 K). We find that the speed of aggregation, based on the aggregation index, is similar, and is determined to leading order by dT. This gives us confidence that the hot-spot temperature anomaly is indeed the main control parameter, not its absolute temperature.

Previous studies showed that the self-aggregation of convective clouds is sensitive to initial conditions so that just by changing initial noise which are small compared to the initial condition, the aggregation onset may delay or hasten. To check the robustness of our results regarding the timing of the onset and the speed of aggregation, we ran two small ensembles of 5 members for dT5R70 and dT5R80 with homogenized radiation, using different initial noises. The ensemble simulations show that the aggregation onset and speed do not vary significantly among the members, in particular the R=80 km simulations are all faster than the R=70 km. This suggests that the aggregation speed is set mostly by the hot-spot forcing, and dependency on the initial conditions is small.

b. Two-box model: Pulled or pushed aggregation?

Here we further investigate the mechanisms involved in the aggregation of the convection in the absence of radiative feedbacks (Figure 6). Given the potential importance of expansion and

strengthening of the dry patch for the onset of convective aggregation (consistent with the drying in Figure 6b), we will interpret the results in light of a conceptual, two-box model with a dry and a moist region, illustrated in Figure 7. In the moist region, there is upward motion in deep convection. In the dry region, there is subsidence and no deep convection (thus no latent heat release). Therefore, given the small horizontal gradients of temperature in the tropics (so-called weak temperature gradient approximation or WTG (Sobel et al. 2001)), to first order the temperature equation for a given pressure level (500 hPa in the following) yields:

$$\frac{\partial T}{\partial t} + \Gamma w^{dry} = Q_{rad} \tag{3}$$

$$\Rightarrow \qquad w^{dry} = \frac{Q_{rad} - \partial T/\partial t}{\Gamma}, \tag{4}$$

where w^{dry} is the (negative) subsidence velocity (m/s), Q_{rad} the (negative) radiative cooling (K/s), and

$$\Gamma = \frac{T}{\theta}\frac{d\theta}{dz} \tag{5}$$

the static stability (θ denotes potential temperature in K). At equilibrium (i.e. $\partial T/\partial t = 0$), there is a balance between subsidence warming and radiative cooling in the dry environment. We nevertheless retain the temperature term $\partial T/\partial t$ in anticipation of w^{dry} that it may be important during the onset of self-aggregation, before equilibrium is reached. Recall that in these simulations without radiative feedback, the radiative cooling rates are homogenized in space, but is allowed to evolve in time.

As stated in the introduction for self-aggregation with radiative feedbacks, the stronger radiative cooling in dry regions compared to the moist regions causes further subsidence drying and generates a circulation that "pushes" the moisture towards the deep convection area (Figure 7). Thus self-aggregation is rather a self-confinement of moisture, as dry regions expand and strengthen, pushing the convection in a small part of the domain in our doubly-periodic geometry. In the

hot-spot aggregation however, the hot-spot increases the convective instability and leads to deep convection localized over the hot-spot. Warmer and moister low level conditions over the hot spot increases the convective instability compare to the environment if we assume that the free troposphere temperature is horizontally homogeneous (Bretherton and Smolarkiewicz 1989). This generates a large-scale circulation with upward motion over the hot-spot and subsidence in its environment, yielding subsidence drying and convectively suppressed conditions in the region surrounding the hot-spot. The moisture is thus "pulled" in the convective region by the large-scale circulation induced by the convective instability over the hot-spot.

The aggregation may be separated into two different phases (Figure 6): the aggregation onset phase where dry regions expand and dry further, and the equilibrium phase when aggregation is well established and the simulation is statistically in equilibrium. The mechanisms which govern aggregation at each of these phases might be different (Muller and Held 2012). For instance, Wing and Emanuel (2014) find that in the onset phase, surface latent heat fluxes act as a positive feedback largely due to enhanced latent heat fluxes in the moist region, while in the equilibrium phase the aggregation is opposed by enhanced surface fluxes in dry regions. Previous studies using the SAM model with homogeneous SST show that the radiative feedback is necessary for both the onset and the maintenance of aggregation, so that homogenizing the radiation profile even after the formation of aggregation leads to a non-aggregated convection. We showed above that a persistent SST anomaly can generate and sustain aggregation even with homogenized radiation. In the following sections we further focus on the hot-spot simulations with homogenized radiation (Figure 6). We analyze first the aggregation processes by considering separately dry and moist regions and by focusing on the aggregation onset phase. The equilibrium state will be addressed later in § 5. We define the onset phase as the time between the beginning of the simulation and the first maximum of the aggregation index. The onset phase varies from less than 10 days to more

than 50 days for the simulations considered in Figure 6 and Table 1. Figure 6b shows that the aggregation index is mostly driven by the *CRH* values in the dry patches ($CRH < 25^{th}$ percentile).

c. The aggregation onset phase

The strength of the subsidence in the dry patch is characterized by its average vertical velocity at 500 hPa ($\overline{W_{500}}^{dry}$). Our hypothesis is that the subsidence strength is correlated with the aggregation onset and time scale. Stronger subsidence outside the hot-spot leads to an enhanced subsidence drying in dry regions, this is an important process that is mostly driven by the positive radiative feedback in the self-aggregation, but it is driven here only by the enhanced vertical motion over the hot-spot (Figure 7). Consistent with this hypothesis, at the beginning of the simulations, the subsidence over the dry patch is larger for larger hot-spots (Figure 8a). This can be interpreted as a very fast response to the convective activity over the hot-spot giving a strong subsidence over the surrounding cold ocean region. This response, much faster for larger hot-spots, is largely due to the fact that the initial conditions of the atmosphere (based on a SST of 300 K) enhanced the convective instability over the hot-spot. This plays a role in the aggregation speed, in a manner that may be exaggerated in regard to a hot-spot formation related, for example, to the diurnal surface temperature warming over an island. In that case, our results suggest that the adjustment is too slow (a few days) for such a diurnal variation to reach an equilibrium. Once the aggregation progresses, for hot-spot radius larger than 70 km, $\overline{W_{500}}^{dry}$ becomes progressively weaker so that by the end of the aggregation onset phase, it becomes even weaker than for simulations without aggregation.

Equation 4 gives a good estimate of the evolution of the actual $\overline{W_{500}}^{dry}$ (Figure 8b) that makes it possible to analyze further the contributions of the radiative cooling term Q_{rad} and of the warming term $\partial T/\partial t$ in the weakening of the subsidence over the dry patch (Figure 8c and 8d). The

difference in the time evolution of the subsidence is largely controlled by the warming term $\partial T/\partial t$ and not by Q_{rad} during the aggregation onset phase. The warming term $\partial T/\partial t$ is large as the domain is adjusting to the warmer condition over the hot-spot. The adjusting time is about 10 days for large hot-spots. We note that this warming term is much smaller if we use atmospheric initial conditions corresponding to the hot-spot temperature. The larger temperature above the hot-spot yields warmer atmospheric temperatures there, which are progressively impressed on the whole domain through compensating subsidence and via propagating gravity waves (Bretherton and Smolarkiewicz 1989). As shown in Figure 8, this effect is stronger for larger hot-spots for which the term $\partial T/\partial t$ decreases dramatically during the aggregation onset phase. For large hot-spots, Q_{rad} is slightly larger at the end of the aggregation onset phase, showing the effect of a well organized dry patch compared to simulations without organized convection.

This moisture "pulling" leading to convective aggregation is associated to different overturning time scales in these simulations, with typically faster aggregation for larger hot-spots. Note however that for R=285 km, the subsidence is found to be slightly smaller compared to R=180 km or R=220 km, in good agreement with a longer aggregation onset phase (Figure 6). For R=285 km, the subsidence is smaller because the potential upward mass flux over the hot-spot is too large to be compensated by subsidence outside of the hot-spot, so that a relatively large part of the hot-spot is included in the subsiding region.

Thus, the aggregation is closely related to the large-scale circulation, as measured by the subsidence velocity in dry regions. The larger fractional area that hot-spot covers, the larger $\overline{W_{500}}^{dry}$ becomes. This can be well seen in Figure 8a.

The decrease of $\overline{W_{500}}^{dry}$ during the aggregation onset phase for large hot-spots is caused by the initial transient warming (Equation 4 and Figure 8c). Eventually, $\overline{W_{500}}^{dry}$ becomes nearly constant in time, as the equilibrium is reached. Then the main balance in dry regions is between subsidence

warming and radiative cooling ($\partial T/\partial t \approx 0$). The warming-induced enhanced static stability (large Γ in Equation 4) reduces the subsidence velocity in aggregating simulations (Figure 8a). Thus the vertical subsiding velocities in dry regions of aggregated simulations become smaller than non-aggregating ones once equilibrium is reached. This is how the expansion and strengthening of the dry patch is halted and equilibrium is reached, despite the stronger radiative cooling rates. This equilibrium phase will be further analyzed in the following section.

5. Equilibrium phase

Here we investigate how the strongest convective cells and updrafts are distributed in the equilibrium phase, and whether the aggregated cluster stays over the hot spot. To study the equilibrium state, we consider a period of 15 days starting at day 35 and ending at day 50 for which the simulations already reached the equilibrium phase (Figure 6), except for a hot-spot of R70 for which we look at the last five days as this period is closer to the equilibrium.

Figure 9 shows *CRH* and W_{500} fields averaged over this period. For $R \leq 65$ km, there is no aggregation visible on the *CRH* field or detected by aggregation index, however W_{500} is much stronger over the hot-spot compared to its environment. For $R = 70$ the aggregation is still on progress. The CRH map of this simulation shows both dry and moist area, however, similar to $R = 60$ and 65, the convection over the hot-spot is much stronger than over the environment. For $R = 80$ km, the convection is not totally centered on the hot-spot for this equilibrium phase. For the largest hot-spots, the region of large *CRH* is well centered on the center of the hot-spots. The concentration of the moist patch over the hot-spot for aggregated simulations is not systematic. In the simulations with interactive radiation (not homogenized in space), the aggregated cluster is indeed not always centered over the hot-spot (Figure 2.b). In fact, once equilibrium is reached in the simulations with radiative feedbacks, the moist patch seems to decouple from the surface.

It does not stay in the same location and can move across the domain. Thus this result that the convection is located over the hot-spot is not robust once radiative feedbacks are accounted for. With radiative feedbacks, whether the convective cluster stays over the hot-spot probably depends on the strength of radiative feedbacks compared to the hot-spot effects.

Despite the large variability of the aggregation index and of the *CRH* pattern among the simulations without radiative feedbacks, maximum values of W_{500} are always located over the hot-spot (with an annular shape for $R \leq 65$ km) during the equilibrium phase (Fig.9). A striking result is that the fractional area of large W_{500} (e.g. $W_{500} > 0.08$ m/s) is relatively independent of the radius of the hot-spot. This region with large W_{500} (Figure 9b) has a fractional area of approximately 10 % for all hot-spot radii.

Figure 10 shows the vertical profiles of the domain mean relative humidity and radiative cooling rates at equilibrium. Simulations with large aggregation index have a drier average profile in agreement with low *CRH* in the dry patch (Fig.6) and with earlier studies of self-aggregation. Average radiative cooling profiles are similar among the simulations which aggregate, with a large radiative cooling rate near the surface. These profiles are consistent with the very dry conditions and strong low-level radiative cooling accompanying aggregation found in earlier studies (Muller and Bony 2015).

6. Conclusions

In this paper, we investigate the role of persistent warm SST anomalies (hot-spots) on the aggregation of deep convective clouds in cloud-resolving simulations. To this end, we perform simulations in radiative-convective equilibrium with SST anomalies of varying size and amplitude, but keeping the domain mean SST constant between simulations. Earlier studies with homogeneous SSTs find that radiative feedbacks are necessary for both the onset and maintenance of a

self-aggregation of the convection for typical tropical temperatures ($\sim$ 300 K). As for previous studies, we find that self-aggregation over homogeneous SSTs is favored at warm temperatures. We also find that the presence of a hot-spot significantly accelerates the aggregation process and extends the range of average SSTs for which aggregation occurs.

We interpret these different behaviors by the fact that the mechanisms for convective aggregation with a hot-spot or with homogeneous SSTs are different. With homogeneous SSTs, the aggregation of convection starts by a strengthening and an expansion of a dry region. Strong radiative cooling in dry regions yields enhanced subsidence that further dries the dry regions and that "pushes" low-level moisture toward the convective region (Figure 7a). In other words, radiatively-driven subsidence inhibits convection in the dry region (Wing et al. 2017; Bretherton et al. 2005; Muller and Held 2012).

With a hot-spot, we find that aggregation (it is no more a self-aggregation since it is forced by the persistent SST anomaly) can occur even in the absence of radiative feedbacks (removed by homogenizing horizontally radiative cooling rates) if the hot-spot is warm and large enough. The hot-spot triggers aggregation by locally increasing the convective instability. Indeed, the warmer and moister conditions at low level over the hot-spot favor deep convection, which brings the atmosphere towards a warmer condition. These warmer temperatures are imprinted over the whole domain through compensating subsidence warming in drier regions and via the propagation of gravity waves (Bretherton and Smolarkiewicz 1989). This subsidence favors further drying in dry regions. This is the positive feedback responsible for the expansion and strengthening of dry regions in hot-spot simulations that aggregate. In other words, the hot-spot "pulls" convection over itself, by generating a large-scale circulation with subsidence outside the hot-spot (Figure 7b).

In our simulations, planetary rotation is neglected so there is no limiting scale (beyond the dissipative scale) for the propagation of waves. So in our doubly-periodic geometry, the subsidence

compensates upward convective motion and is thus potentially stronger when the fractional area of the hot-spot increases. In particular, for a given hot-spot radius, the subsidence is sensitive to the domain size. This highlights the importance of using large domains when investigating island convection in similar non-rotating doubly-periodic settings, in order to either avoid or control the triggering of self-aggregation feedbacks. In particular, the doubly-periodic confinement of the large scale circulation induced by surface heterogeneities may explain the non-monotonic responses of precipitation to an island found in idealized simulations of convection over tropical islands. In such simulations, precipitation is found to increase and then decrease as a function of island radius holding the domain size fixed. Our results suggest that the large-scale circulation induced by the island may be impacted by the domain size if the domain is not large enough compared to the island.

In reality, with planetary rotation, the scale of the large-scale circulation induced by SST anomalies is likely determined by the Rossby radius of deformation. Our results suggest that for a large enough fractional area of SST anomalies compared to this large-scale circulation, self-aggregation feedbacks could play a role in organizing deep convection over SST anomalies. In the ocean, SST anomalies of the size studied here ($\mathcal{O}$(100 km)) are not uncommon, taking the form of mesoscale eddies (Chelton 2011). Their contribution to convective organization deserves further investigation. Finally, these findings raise questions on the organization of deep convection over tropical islands, e.g. of the maritime continent. There, a strong diurnal cycle further interacts with aggregation feedbacks and tendencies (Cronin et al. (2014)). Our results show that the adjustment of the average temperature profile to the hot-spot SST anomaly takes a few days for large hot-spots, which is very slow compared to diurnal variability of surface temperature over tropical islands (reaching to a maximum typically in 6h between sunrise and noon). Therefore, the atmosphere, and the convective aggregation pattern itself, will not have time to fully adjust before the island

starts cooling down in the afternoon. Further work is needed to investigate the implication of our results on the diurnal cycle of convection over tropical islands.

Acknowledgments. This project has received funding from the Marie - Sklodowska Curie Actions (MSCA) under the European Union's Horizon 2020 research and innovation programme (grant agreement no 675675). The authors gratefully acknowledge funding from the French national program Les Enveloppes Fluides et l'Environnement (LEFE) of Institut National des Sciences de l'Univers (INSU), and from the program Paris Sciences et Lettres PSL-NYU (ANR-10-IDEX-0001-02). Finally, the authors would like to thank Kerry Emanuel and two anonymous reviewers for their useful comments about this work.

References

Abbot, D. S., 2014: Resolved snowball earth clouds. *J. Climate*, **27 (12)**, 4391–4402, doi:10.1175/JCLI-D-13-00738.1.

Bellenger, H., J. Duvel, M. Lengaigne, and P. Levan, 2009: Impact of organized intraseasonal convective perturbations on the tropical circulation. *Geophys. Res. Lett.*, **36**, L16 703, doi:10.1029/2009GL039584.

Beringer, J., and N. Tapper, 2002: Surface energy exchanges and interactions with thunderstorms during the maritime continent thunderstorm experiment (mctex). *J. Geophys. Res.*, **107 (D21)**, AAC 3–1–AAC 3–13, doi:10.1029/2001JD001431.

Bretherton, C. S., P. N. Blossey, and M. Khairoutdinov, 2005: An energy-balance analysis of deep convective self-aggregation above uniform SST. *J. Atmos. Sci.*, **62 (12)**, 4273–4292, doi:10.1175/JAS3614.1.

569 Bretherton, C. S., and P. K. Smolarkiewicz, 1989: Gravity waves, compensating subsidence
570 and detrainment around cumulus clouds. *J. Atmos. Sci.*, **46 (6)**, 740–759, doi:10.1175/
571 1520-0469(1989)046⟨0740:GWCSAD⟩2.0.CO;2.

572 Chelton, D., 2011: Global observations of nonlinear mesoscale eddies. *Prog. Oceanogr.*, **91 (2)**,
573 167 – 216, doi:https://doi.org/10.1016/j.pocean.2011.01.002.

574 Collins, W. D., and Coauthors, 2006: The formulation and atmospheric simulation of the com-
575 munity atmosphere model version 3 (cam3). *J. Climate*, **19 (11)**, 2144–2161, doi:10.1175/
576 JCLI3760.1.

577 Coppin, D., and S. Bony, 2015: Physical mechanisms controlling the initiation of convective
578 self-aggregation in a general circulation model. *J. Adv. Model. Earth Syst.*, **7 (4)**, 2060–2078,
579 doi:10.1002/2015MS000571.

580 Cronin, T., K. A. Emanuel, and P. Molnar, 2014: Island precipitation enhancement and the diurnal
581 cycle in radiative-convective equilibrium. *Quart. J. Roy. Meteor. Soc.*, **141**, doi:10.1002/qj.2443.

582 Crook, N. A., 2001: Understanding hector: The dynamics of island thunderstorms. *Mon. Wea.*
583 *Rev.*, **129**, 1550–1563, doi:10.1175/1520-0493(2001)129⟨1550:UHTDOI⟩2.0.CO;2.

584 Daleu, C. L., R. S. Plant, and S. J. Woolnough, 2017: Using the weak-temperature gradient ap-
585 proximation to evaluate parameterizations: An example of the transition from suppressed to
586 active convection. *J. Adv. Model. Earth Syst.*, **9 (6)**, 2350–2367, doi:10.1002/2017MS000940.

587 Emanuel, K. A., A. A. Wing, and E. M. Vincent, 2014: Radiative-convective instability. *J. Adv.*
588 *Model. Earth Syst.*, **6 (1)**, 75–90, doi:10.1002/2013MS000270.

589 Grabowski, W. W., 2006: Impact of explicit atmosphereocean coupling on MJO-like coherent
590 structures in idealized aquaplanet simulations. *J. Atmos. Sci.*, **63 (9)**, 2289–2306, doi:10.1175/
591 JAS3740.1.

592 Grabowski, W. W., and M. W. Moncrieff, 2001: Large-scale organization of tropical convection
593 in two-dimensional explicit numerical simulations. *Quart. J. Roy. Meteor. Soc.*, **127 (572)**, 445–
594 468, doi:10.1002/qj.49712757211.

595 Gray, W., and R. Jacobson, 1977: Diurnal variation of deep cumulus convection. *Mon. Wea. Rev.*,
596 **105**, 1171–1187, doi:10.1175/1520-0493(1977)105⟨1171:DVODCC⟩2.0.CO;2.

597 Holloway, C. E., 2017: Convective aggregation in realistic convective-scale simulations. *J. Adv.*
598 *Model. Earth Syst.*, **9 (2)**, 1450–1472, doi:10.1002/2017MS000980.

599 Houze, R. A., Jr., 2004: Mesoscale convective systems. *Rev. Geophys.*, **42 (4)**, RG4003, doi:
600 10.1029/2004RG000150.

601 Khairoutdinov, M. F., and K. A. Emanuel, 2010: Aggregated convection and the regulation of
602 tropical climate. *Preprints, 29th conference on Hurricanes and Tropical Meteorology, Tucson,*
603 *AZ, Amer. Meteor. Soc.*, **P2.69**.

604 Khairoutdinov, M. F., and D. A. Randall, 2003: Cloud resolving modeling of the ARM summer
605 1997 IOP: Model formulation, results, uncertainties, and sensitivities. *J. Atmos. Sci.*, **60 (4)**,
606 607–625, doi:10.1175/1520-0469(2003)060⟨0607:CRMOTA⟩2.0.CO;2.

607 Kuang, Z., 2012: Weakly forced mock walker cells. *J. Atmos. Sci.*, **69**, 2759–2786, doi:10.1175/
608 JAS-D-11-0307.1.

609 Mapes, B., and R. Neale, 2011: Parameterizing convective organization to escape the entrainment
610 dilemma. *J. Adv. Model. Earth Syst.*, **3 (2)**, doi:10.1029/2011MS000042.

Mapes, B. E., 2001: Water's two height scales: The moist adiabat and the radiative troposphere. *Quart. J. Roy. Meteor. Soc.*, **127 (577)**, 2353–2366, doi:10.1002/qj.49712757708.

Muller, C. J., 2013: Impact of convective organization on the response of tropical precipitation extremes to warming. *J. Climate*, **26**, 5028–5043, doi:10.1175/JCLI-D-12-00655.1.

Muller, C. J., and S. Bony, 2015: What favors convective aggregation and why? *Geophys. Res. Lett.*, **42 (13)**, 5626–5634, doi:10.1002/2015GL064260.

Muller, C. J., and I. M. Held, 2012: Detailed investigation of the self-aggregation of convection in cloud-resolving simulations. *J. Atmos. Sci.*, **69**, 2551–2565, doi:10.1175/JAS-D-11-0257.1.

Muller, C. J., and P. A. O'Gorman, 2011: An energetic perspective on the regional response of precipitation to climate change. *Nature Climate Change*, **1 (5)**, 266–271.

Muller, C. J., P. A. O'Gorman, and L. E. Back, 2011: Intensification of precipitation extremes with warming in a cloud-resolving model. *J. Climate*, **24 (11)**, 2784–2800, doi:10.1175/2011JCLI3876.1.

Pauluis, O., and I. M. Held, 2002: Entropy budget of an atmosphere in radiative–convective equilibrium. part i: Maximum work and frictional dissipation. *J. Atmos. Sci.*, **59 (2)**, 125–139, doi:10.1175/1520-0469(2002)059⟨0140:EBOAAI⟩2.0.CO;2.

Qian, J.-H., 2008: Why precipitation is mostly concentrated over islands in the maritime continent. *J. Atmos. Sci.*, **65 (4)**, 1428–1441, doi:10.1175/2007JAS2422.1.

Ramsay, H. A., and A. H. Sobel, 2011: Effects of relative and absolute sea surface temperature on tropical cyclone potential intensity using a single-column model. *J. Climate*, **24 (1)**, 183–193, doi:10.1175/2010JCLI3690.1.

Romps, D. M., 2010: A direct measure of entrainment. *J. Atmos. Sci.*, **67 (6)**, 1908–1927, doi: 10.1175/2010JAS3371.1.

Ruppert, J., and C. Hohenegger, 2018: Diurnal circulation adjustment and organized deep convection. *J. Climate*, doi:10.1175/JCLI-D-17-0693.1.

Sobel, A. H., and C. S. Bretherton, 2000: Modeling tropical precipitation in a single column. *J. Climate*, **13 (24)**, 4378–4392, doi:10.1175/1520-0442(2000)013⟨4378:MTPIAS⟩2.0.CO;2.

Sobel, A. H., C. D. Burleyson, and S. E. Yuter, 2011: Rain on small tropical islands. *J. Geophys. Res.*, **116 (D8)**, doi:10.1029/2010JD014695.

Sobel, A. H., J. Nilsson, and L. M. Polvani, 2001: The weak temperature gradient approximation and balanced tropical moisture waves. *J. Atmos. Sci.*, **58**, 23, doi:10.1175/1520-0469(2001) 058⟨3650:TWTGAA⟩2.0.CO;2.

Sugimoto, S., K. Aono, and S. Fukui, 2017: Local atmospheric response to warm mesoscale ocean eddies in the kuroshiooyashio confluence region. *Scientific Reports*, **7 (11871)**.

Tan, J., C. Jakob, W. B. Rossow, and G. Tselioudis, 2015: Increases in tropical rainfall driven by changes in frequency of organized deep convection. *Nature*, **519 (7544)**, 451, doi:10.1038/ nature14339.

Tobin, I., S. Bony, and R. Roca, 2012: Observational evidence for relationships between the degree of aggregation of deep convection, water vapor, surface fluxes, and radiation. *J. Climate*, **25**, 6885–6904, doi:10.1175/JCLI-D-11-00258.1.

Tompkins, A. M., 2001a: Organization of Tropical Convection in Low Vertical Wind Shears: The Role of Cold Pools. *J. Atmos. Sci.*, **58**, 16501672, doi:10.1175/1520-0469(2001)058⟨1650: OOTCIL⟩2.0.CO;2.

Tompkins, A. M., 2001b: Organization of tropical convection in low vertical wind shears: The role of water vapor. *J. Atmos. Sci.*, **58 (6)**, 529–545, doi:10.1175/1520-0469(2001)058⟨0529:OOTCIL⟩2.0.CO;2.

Tompkins, A. M., and G. C. Craig, 1998: Radiative-convective equilibrium in a three-dimensional cloud-ensemble model. *Quart. J. Roy. Meteor. Soc.*, **124**, 2073–2097, doi:10.1002/qj.49712455013.

Wang, S., and A. H. Sobel, 2011: Response of convection to relative sea surface temperature: Cloud-resolving simulations in two and three dimensions. *J. Geophys. Res.*, **116 (D11)**, doi:10.1029/2010JD015347.

Wang, S., and A. H. Sobel, 2017: Factors controlling rain on small tropical islands: Diurnal cycle, large-scale wind speed, and topography. *J. Atmos. Sci.*, **74 (11)**, 3515–3532, doi:10.1175/JAS-D-16-0344.1.

Wing, A., K. Emanuel, C. Holloway, and C. Muller, 2017: Convective self-aggregation in numerical simulations: A review. *Surv. Geophys.*, **38 (6)**, 1173–1197, doi:10.1007/978-3-319-77273-8_1.

Wing, A. A., and T. W. Cronin, 2016: Self-aggregation of convection in long channel geometry. *Quart. J. Roy. Meteor. Soc.*, **142 (694)**, 1–15, doi:10.1002/qj.2628.

Wing, A. A., and K. A. Emanuel, 2014: Physical mechanisms controlling self-aggregation of convection in idealized numerical modeling simulations. *J. Adv. Model. Earth Syst.*, **6 (1)**, 59–74, doi:10.1002/2013MS000269.

Zuidema, P., G. Torri, and C. Muller, 2017: Precipitation-induced atmospheric cold pools over oceans and their interactions with the larger-scale environment. *Surv. Geophys.*, **38 (6)**, 1283–1305, doi:10.1007/s10712-017-9447-x.

LIST OF TABLES

TABLE 1. List of all the simulations with homogenized radiation. Shown are the hot-spot radius, the fractional area covered by it (with one digit for values below 10 %), its temperature anomaly (dT), ocean temperature and domain mean SST.

HS Radius (km)	$A^{hs}/(A^{env}+A^{hs})(\%)$	dT (K)	SST^{env} (K)	$\overline{SST}$ (K)
60	3.4	5	299.83	300
65	4.0	5	299.80	300
70	4.6	5	299.77	300
80	6.1	5	299.69	300
80	6.1	3	299.81	300
180	31	5	298.46	300
220	46	5	297.70	300
285	77	5	296.15	300

LIST OF FIGURES

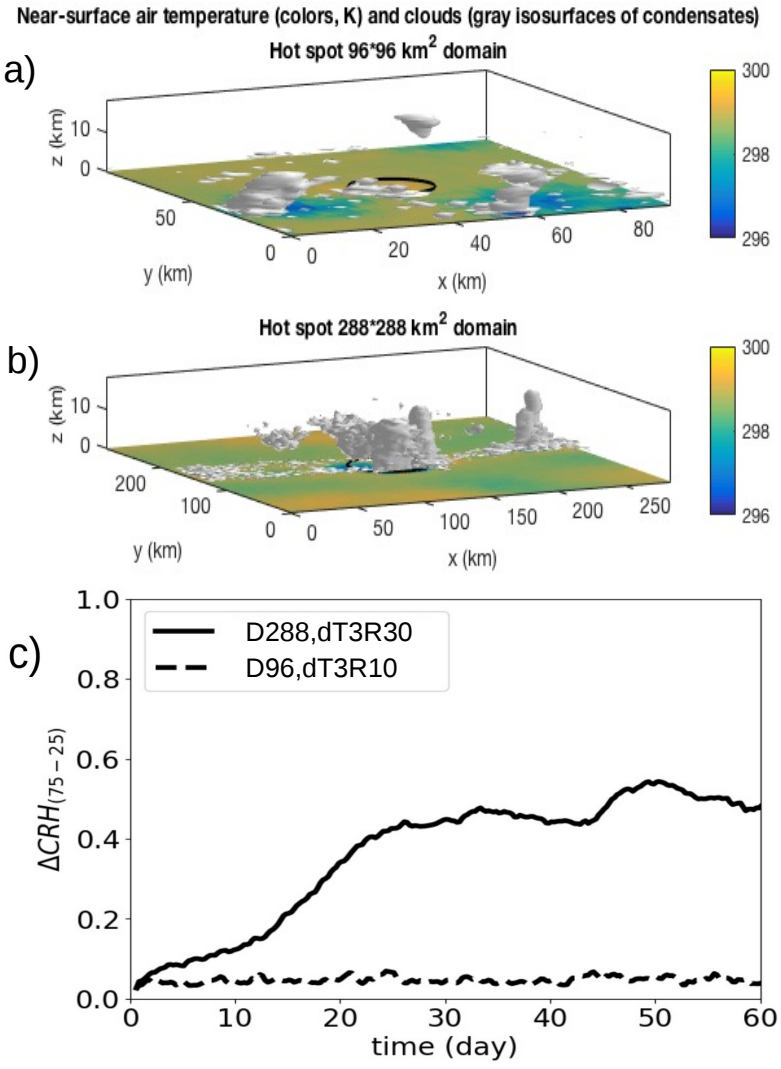

724 FIG. 1. Snapshots of near-surface air temperature (colors, K) and cloud water (grey shades) from two simula-
725 tions with a hot-spot in the center of the domain (circle) for (a) a domain size 96*96km^2 and (b) 288*288 km^2.
726 (c) Time evolution of the aggregation index for those two simulations.

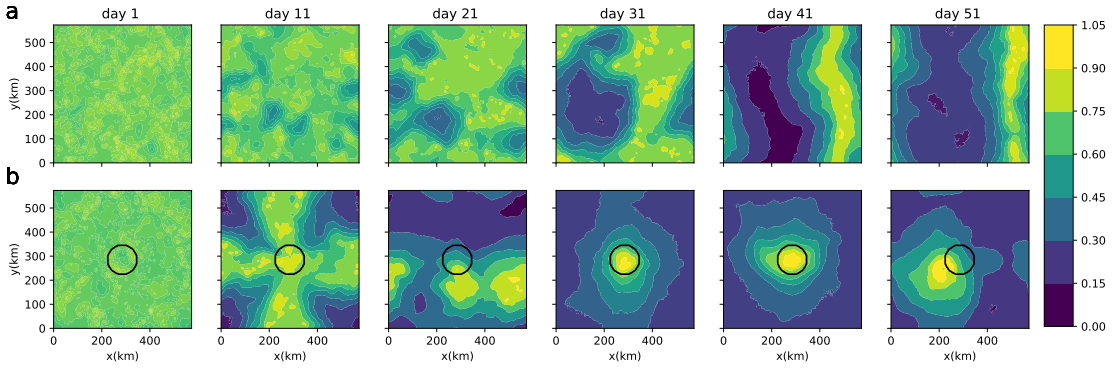

FIG. 2. Snapshots of *CRH* for simulations with (a) a uniform surface temperature and (b) a hot-spot with a SST anomaly of 5 K and a radius of 60 km. The black circle shows the hot-spot boundary. For both simulations the domain average SST is 300K and the domain size is 576*576 km^2

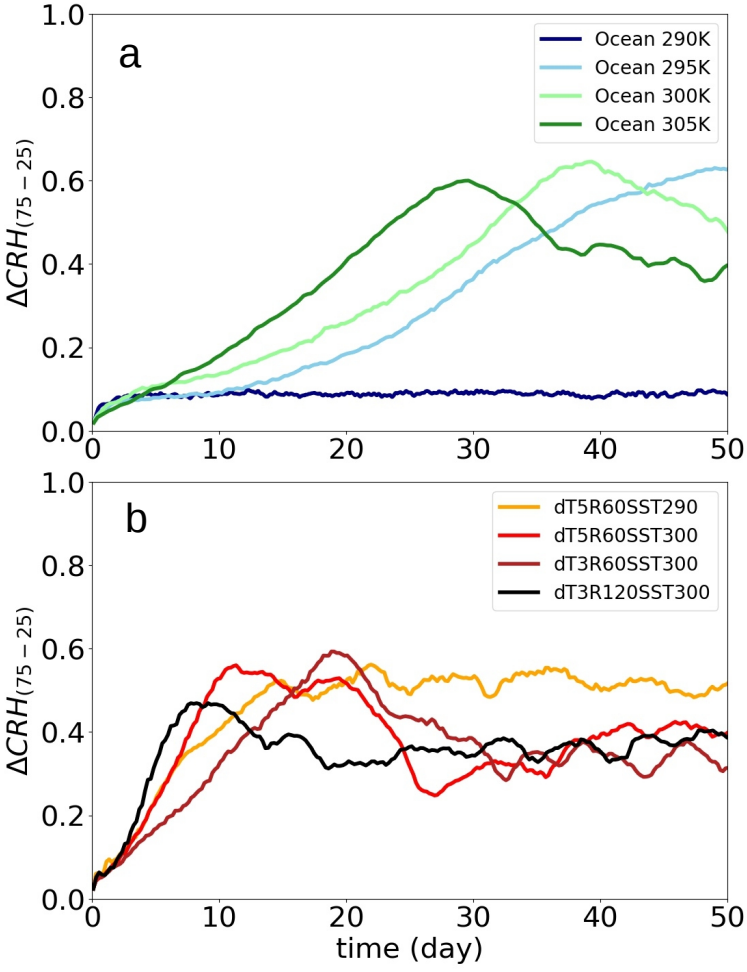

730 FIG. 3. Time evolution of the aggregation index for simulations with full radiative feedback for: (a) sim-
731 ulations with a uniform surface temperature (referred to as "Ocean" see §2b for a detailed description of the
732 simulations); (b) simulations with a hot-spot of different sizes and SST anomalies.

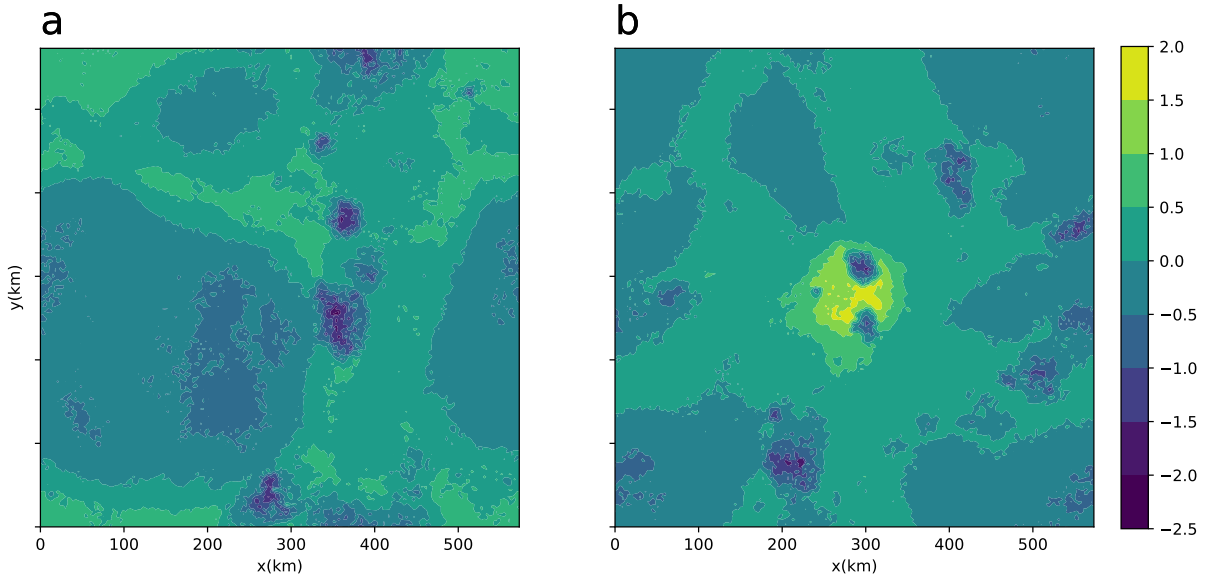

FIG. 4. θv anomaly averaged over the boundary layer (from surface to 1000 m) for a) day 31 of ocean experiment at 300 K , b) day 11 of Hot-spot experiment dT5R60 and mean SST=300 K.

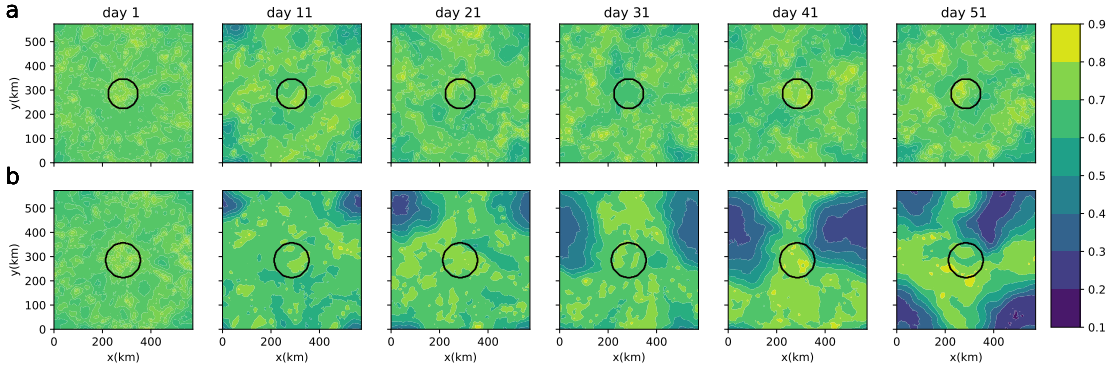

FIG. 5. Snapshots of *CRH* for hot-spot simulations with homogenized radiation for: (a) SST anomaly of 5 K and a radius of 60 km and (b) SST anomaly of 5 K and a radius of 70 km. The black circle shows the hot-spot boundary. For both simulations, the domain average SST is 300 K and the domain size is 576*576 km^2.

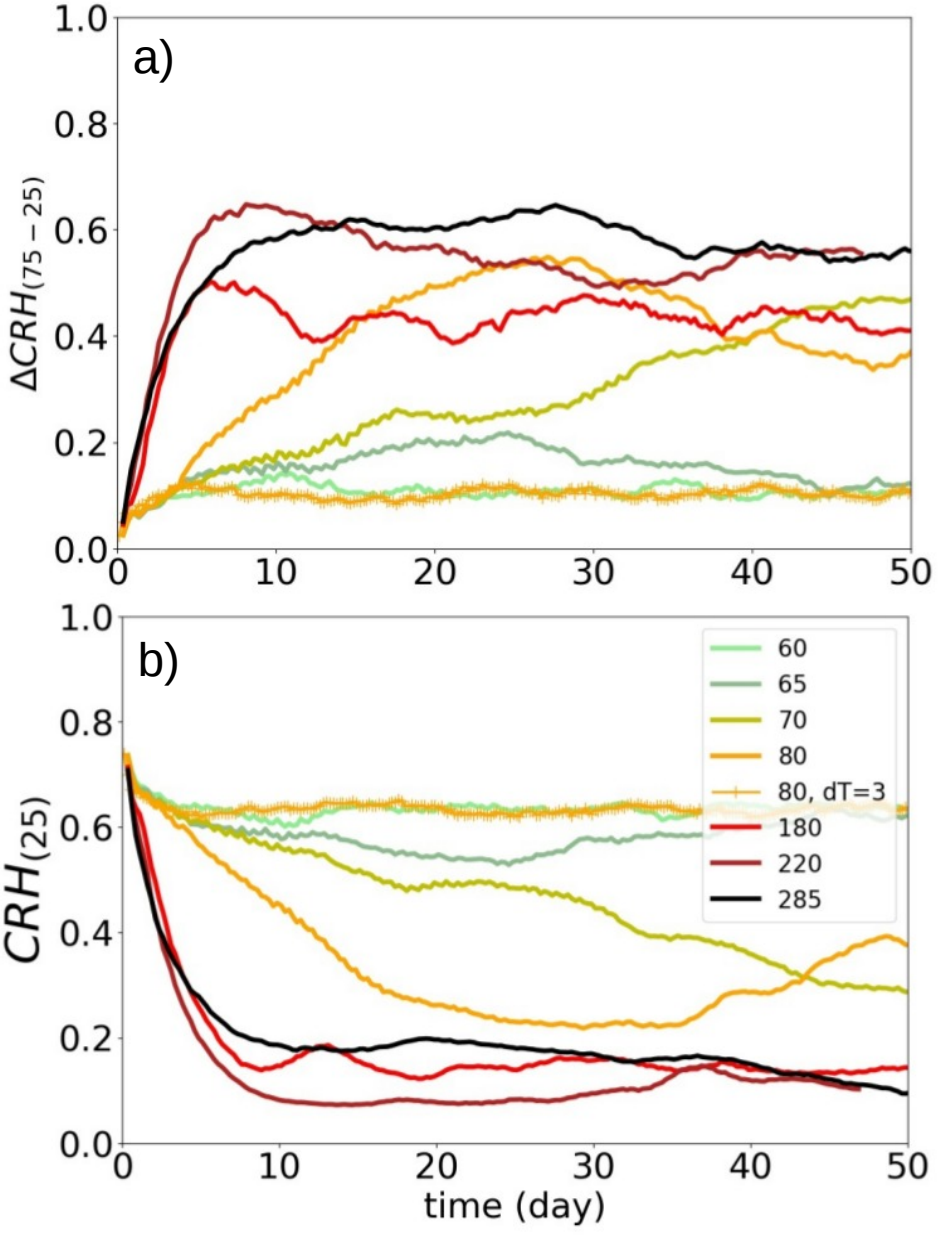

738 FIG. 6. Time evolution of (a) the aggregation index and (b) *CRH* averaged over driest quartile for different
739 hot-spot radius for simulations with homogenized radiation. All the simulations have a domain size of 576*576
740 km^2 and a hot-spot SST anomaly of 5 K except for one simulation with a radius of 80 km and a SST anomaly
741 of 3 K.

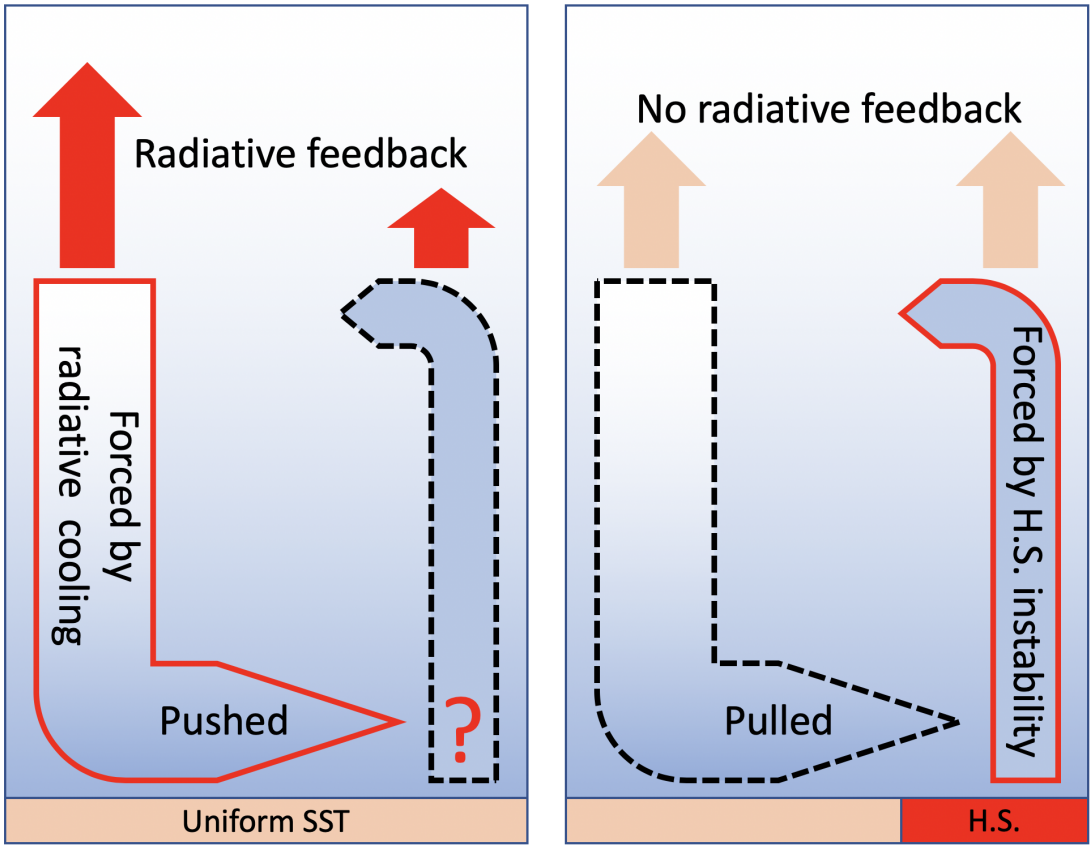

FIG. 7. Schematic two-box model representing either a self-aggregation by radiative feedbacks or an aggregation forced by a hot-spot induced circulation. (a) Self-aggregation by radiative feedbacks is caused by a progressive expansion of a dry subsidence region under the effect of a strong radiative cooling, "pushing" the low-level moisture toward a constricted moist and warm convective region. (b) The aggregation is due to the large-scale circulation induced by the hot-spot persistent SST anomaly, "pulling" the moisture toward the warm anomaly.

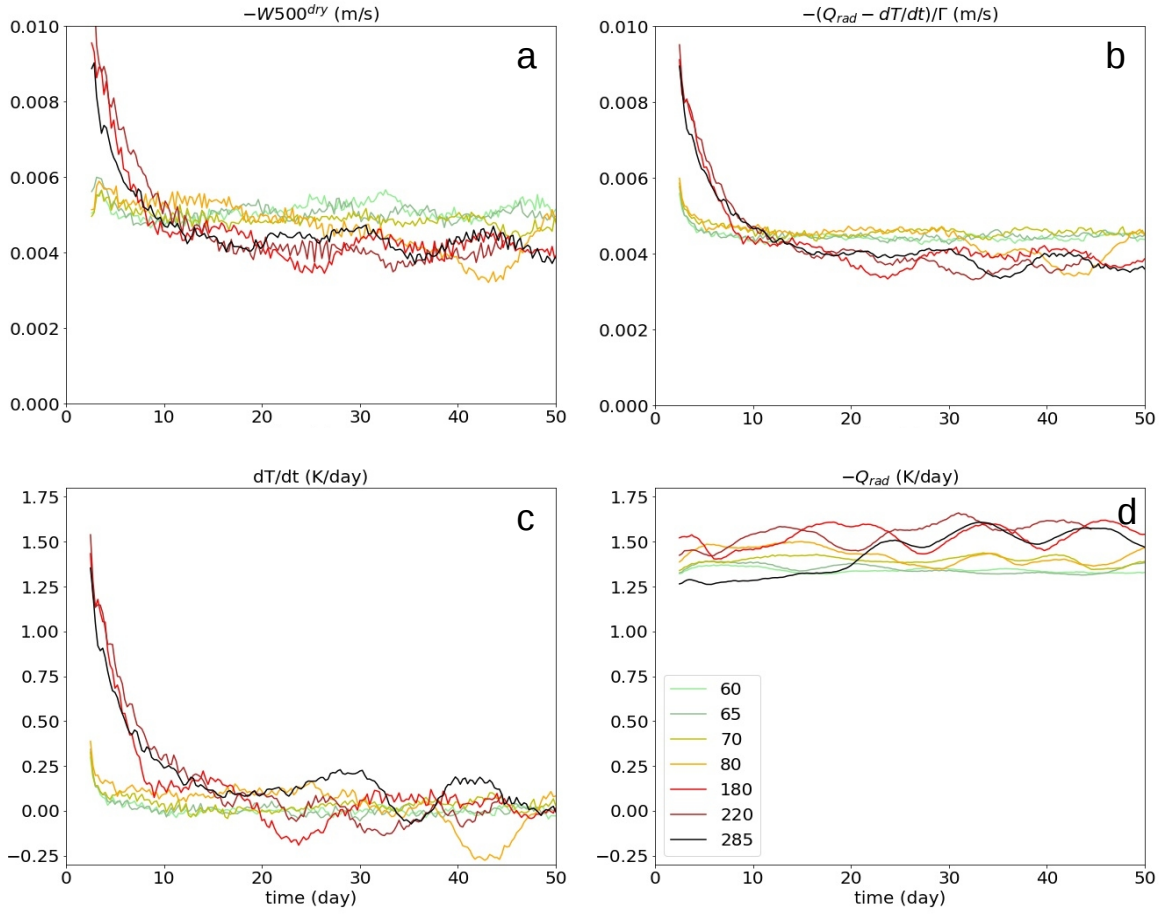

748 FIG. 8. Time evolution of atmospheric parameters at 500 hPa averaged over the dry patch for different hot-
749 spot sizes: (a) vertical velocity; (b) the right hand side of Equation 4; c) the time derivative of temperature and;
750 (d) radiative cooling. The domain average SST is 300 K and the domain size is 576*576 km^2.

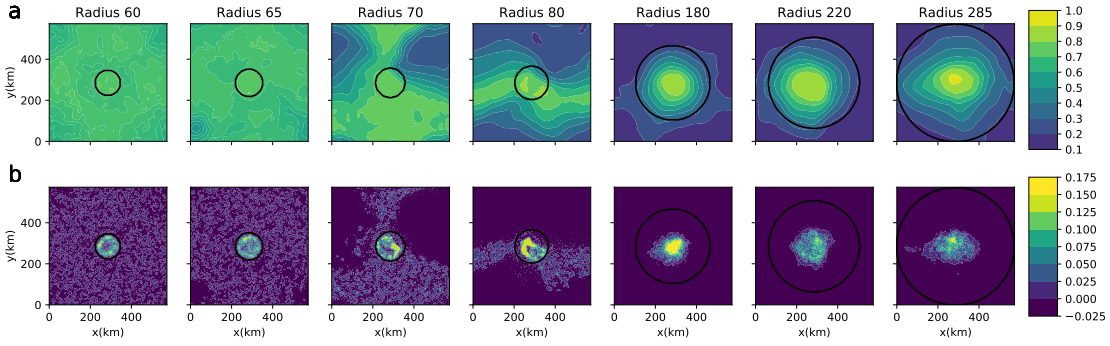

751 FIG. 9. (top) *CRH* and (bottom) W500 (m/s) averaged between day 35 and day 50 of the simulation for hot-
752 spot of different sizes. The domain average SST is 300K, the hot-spot SST anomaly is 5 K and the domain size
753 is 576*576 km^2. The black circle shows the hot-spot.

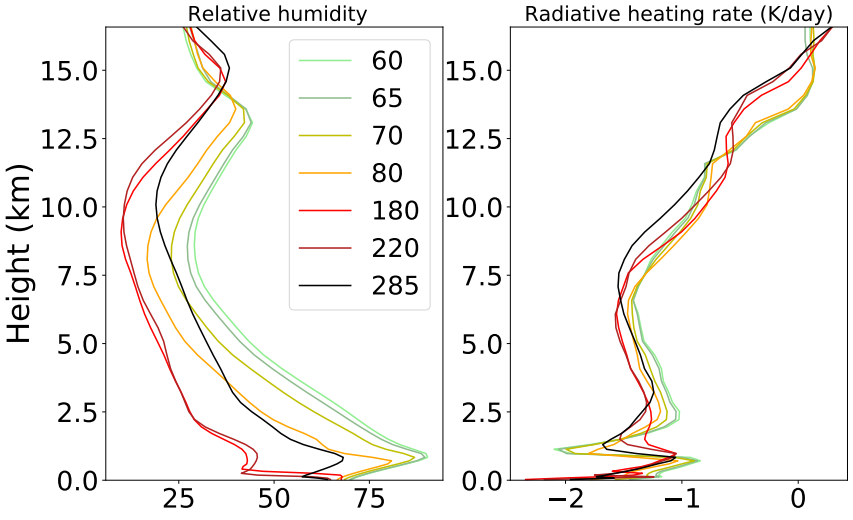

754 FIG. 10. Domain average vertical profiles averaged between day 35 and day 50 of the simulation for hot-spot
755 of different sizes. The domain average SST is 300 K, the hot-spot SST anomaly is 5 K and the domain size is
756 576*576 km^2.